https://ntrs.nasa.gov/search.jsp?R=19830012435 2020-03-21T04:02:55+00:00Z

General Disclaimer

One or more of the Following Statements may affect this Document

- This document has been reproduced from the best copy furnished by the organizational source. It is being released in the interest of making available as much information as possible.

- This document may contain data, which exceeds the sheet parameters. It was furnished in this condition by the organizational source and is the best copy available.

- This document may contain tone-on-tone or color graphs, charts and/or pictures, which have been reproduced in black and white.

- This document is paginated as submitted by the original source.

- Portions of this document are not fully legible due to the historical nature of some of the material. However, it is the best reproduction available from the original submission.

Produced by the NASA Center for Aerospace Information (CASI)

AERODYNAMICS & TURBULENCE LABORATORY

CULLEN COLLEGE OF ENGINEERING

(NASA-CR-170015) THE WHISTLER NOZZLE EFFECTMENCN (Houston Univ.) 36 p
HC A03/MF A01 CSCL 20A

N83-20706

Unclas
G3/71 03092

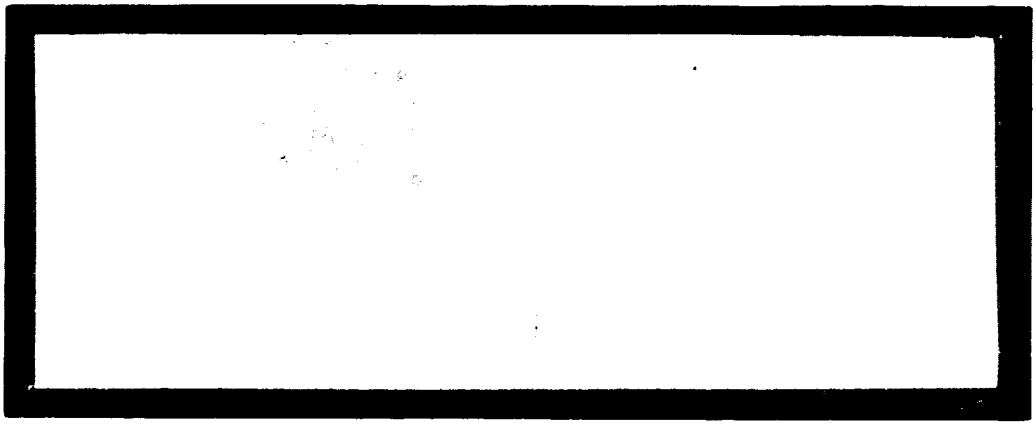

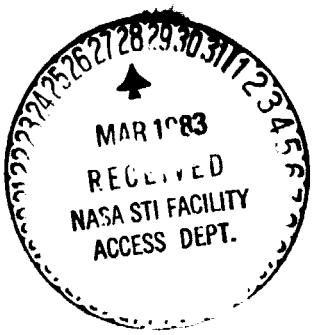

UNIVERSITY OF HOUSTON

HOUSTON ● TEXAS 77004

THE 'WHISTLER NOZZLE' PHENOMENON

Report FM-15

By A.K.M.F. Hussain and M.A.Z. Hasan

Department of Mechanical Engineering
University of Houston
Houston, Texas 77004

October, 1982

Funded by

The NASA Lewis Research Center under Grant NAG-3-198

The 'Whistler Nozzle' Phenomenon

By A. K. M. F. Hussain and M. A. Z. Hasan
Department of Mechanical Engineering
University of Houston, Texas 77004

Abstract

The 'whistler nozzle' is a simple device which can induce jet self-excitations of controllable amplitudes and frequencies and appears highly promising for many applications involving turbulent transport, combustion and aerodynamic noise. This paper documents the characteristics of this curious phenomenon for different values of the controlling parameters and attempts to explain the phenomenon. It is shown that the whistler excitation results from the coupling of two independent resonance mechanisms: shear-layer tone resulting from the impingement of the pipe-exit shear layer on the collar lip, and organ-pipe resonance of the pipe-nozzle. The crucial role of the shear-layer tone in driving the organ-pipe resonance is proven by reproducing the event in pipe-ring and pipe-hole configurations in the absence of the collar. It is also shown that this phenomenon is the strongest when the self-excitation frequency matches the 'preferred mode' of the jet.

The 'whistler nozzle' phenomenon occurs for both laminar and turbulent initial boundary layers; the excitation can be induced without the pipe-nozzle (say, by ring or hole tone) when the exit flow is laminar but not when it is turbulent. Unlike in the shear-layer tone and jet tone phenomena, where successive stages overlap, adjacent stages of the whistler nozzle excitation are separated by 'dead zones' where the conditions for both resonance mechanisms cannot be simultaneously met. Also, unlike in the shear-layer and jet tones, the whistler frequency cannot be varied continuously by changing the speed. Since the phenomenon is the coupling of two resonance mechanisms, the frequency data appear to defy a simple nondimensional representation for the entire range of its operation. Reasonable collapse of data is achieved, however, when the exit momentum thickness is used as a length scale, thus emphasizing the role of the shear-layer tone in the phenomenon.

1. Introduction

In an attempt to explore turbulence augmentation and suppression as well as the role of the large-scale coherent structures and their interactions like tearing and pairing in jet noise and mixing, we were interested in methods of

inducing controlled excitations in the jet. The 'whistler nozzle' presented itself as an attractive possibility because of its amazingly simple configuration, requirement of no external power, and ability to induce self-sustained excitation of controllable amplitudes and frequencies over wide ranges.

The device consists of a round tail-pipe attached to the downstream end of a jet nozzle and an axisymmetric collar sliding over the pipe (figure 1a). As the collar is pulled downstream (i.e., the collar length L_c projecting beyond the pipe is increased), a loud pure tone abruptly appears; (the tone is audible in air at velocities as low as $15ms^{-1}$). This is called the first stage. With increasing L_c, the tone increases in amplitude, reaches a maximum, decreases and then disappears. With a further increase in L_c, the tone reappears. This is the second stage, and so on. The tone frequency and amplitude depend on the pipe-nozzle length L_p, collar length L_c, step height h (i.e., the difference between the inner radii of the nozzle and the collar), jet exit speed U_e, and jet diameter D.

Hill & Greene (1977) appear to be the first to have discovered whistler nozzle excitation, but they were unable to explain the phenomenon or find any relationship between the controlling parameters. The motivation for the present study was to document the whistler nozzle behavior as a function of the controlling parameters, to explain the phenomenon and to validate the explanation via additional experiments in modified configurations (figures 1b,c) without the collar. The phenomenon was explored in low-speed axisymmetric air jet facilities available in our laboratory. The effects of the self-sustained excitation on the axisymmetric free jet emerging from the whistler nozzle have been discussed previously (see Hasan & Hussain 1982, hereinafter referenced as I). Measurements up to 60 diameters showed that the whistler nozzle excitation produces a large increase in the turbulence intensity in the near field of the jet, while it increases the spread and decay rate for the entire x-range of measurement. For further details see I, which complements the results reported here.

(a) The shear-layer tone phenomenon: If an object intercepts a laminar free shear layer, the shear layer can be set into oscillation, depending on the speed U_e and the distance b of the object from the lip. The oscillation can produce discrete audible tones like the jet tone at even fairly low speeds, especially with a sharp edge. As b is increased from zero, a tone abruptly appears at a frequency which decreases with increasing b. With further increase in b, the tone jumps back to a higher frequency. The average

frequency remains the same at successive stages and is the instability frequency of the shear layer stabilized by feedback from the impinging edge. The frequencies in the different stages show collapse when non-dimensionalized by U_e and the exit momentum thickness θ_e. For further details, see Hussain and Zaman (1978), hereinafter referenced as HZ.

2. Apparatus and Procedure

The experiments have been carried out in two axisymmetric air jet facilities with nozzle diameters D=2.54 cm and 7.62 cm. The 2.54 cm jet facility has been described by Zaman & Hussain (1980). The D=2.54 cm pipe is attached to the settling chamber via an ASME nozzle (see I). Data with the 7.62 cm nozzle were obtained in a large jet of 27 cm diameter. The transition to the D=7.62 cm pipe occurs through an ASME nozzle. Additional details of the facility were given by Husain & Hussain (1979).

The centerline longitudinal turbulence intensity at the inlet end of the pipe is about 0.25% for each facility. For the 2.54 cm jet, data were taken with six different L_p's (7.62 cm, 15.24 cm, 30.48 cm, 45.72 cm, 60.96 cm, and 91.44 cm) and two values of h(0.3175 cm and 0.635 cm). Unless otherwise stated, data presented for the 2.54 cm nozzle are for U_e=36ms^{-1} corresponding to the jet Reynolds number Re_D(=$U_eD/$) of 6.2x10^4. For D=7.62 cm, data were taken with two L_p's (30.48 cm and 60.96 cm) at U_e values of 36ms^{-1}, 45ms^{-1} and 60ms^{-1}. The corresponding values of Re_D were: 1.85x10^5, 2.3x10^5 and 3.1x10^5, respectively. For D = 7.62 cm, only one step height h(=0.635 cm) was investigated.

A standard tungsten hot-wire of 4μm diameter operated at an overheat ratio of 0.4 by a linearized (DISA) constant temperature anemometer was used to obtain the data. Most of the data were obtained with a backlash-free traversing mechanism operated by stepping motors, which were controlled on-line by the laboratory computer (HP2000S). The frequency spectra were obtained with a real-time spectrum analyzer (Spectrascope model SD335). The phase of the disturbance signal was measured with a PAR lock-in amplifier; the reference signal was obtained from the flow by bandpassing the velocity signal in the near field of the excited jet.

Note that the origin of the co-ordinates is located at the pipe exit center; x increases in the downstream direction and y increases radially.

3. Results and Discussion

3.1 General Characteristics:

For the 2.54 cm nozzle, unless otherwise specified, data for two L_p's representing two distinctly different initial conditions (i.e., flow charac-

teristics at the pipe exit) will be presented in this paper. These are: L_p=15.24 cm which has a laminar exit boundary layer and L_p=30.48 cm which has a transitional exit boundary layer. For D=2.54 cm, data for longer pipes having turbulent exit boundary layers are not included because all the 7.62 cm diameter pipes have turbulent exit boundary layers.

Even though a large number of measures can be used to define the initial condition, the mean velocity and longitudinal fluctuation intensity profiles and the u-spectrum in the exit boundary layer can be regarded as adequate identifiers of the initial condition. The initial condition can be classified into four groups: laminar, nominally laminar, highly disturbed and fully-developed turbulent (for details see Hussain 1980). Both laminar and nominally laminar cases, identified by the agreement of the mean velocity profile with the Blasius profile, are grouped together in this study and termed 'laminar' for the sake of simplicity. For initially turbulent boundary layer cases, the mean velocity profile had the characteristic logarithmic and wake regions in the universal (U^+,y^+) coordinates, the wake strength agreed with that expected for the corresponding value of Re_θ (Coles 1962), the longitudinal velocity fluctuation intensity profile agreed with that of the flat plate, and the longitudinal velocity spectrum $\phi_u(f)$ was broadband (typically over the frequency range 0-4kHz) without any spectral peaks.

Based on exploratory tests, the phenomenon was inferred by us to be an organ-pipe resonance of the pipe-nozzle triggerred by the shear-layer tone, which is produced by the impingement of the shear layer from the pipe exit on the collar lip. Detailed data discussed in the following further affirm our explanation.

(a) Minimum Collar Length: If the whistler phenomenon involves a shear-layer tone, then there should be a minimum collar length L_{cmin} below which no excitation will take place. This is typical of the shear-layer tone and the jet tone phenomena (HZ; Karamcheti et al. 1969; Rockwell & Naudasher 1979). The L_{cmin} value depends on L_p as well as h. Table 1a shows the values of L_{cmin} for a few cases. With higher values of h, L_{cmin} increases, since the collar has to be longer in order for its lip to intercept the shear-layer and thus induce the shear-layer tone via feedback. Note that for the laminar case (L_p = 15.24 cm), the value of L_{cmin} is proportional to h. At a lower frequency (and hence longer wavelength), the shear-layer roll-up length should be longer, and thus, the length required for vortex impingement and feedback to sustain the shear-layer tone should be higher also.

Since the excitation frequency decreases with increasing L_p, higher L_p gives higher L_{cmin} (table 1a).

(c) Nature of the Excitation: Figure 2 shows hot-wire traces at the pipe exit centerline for a few representative excitation cases covering different stages and L_p's for the 2.54 cm nozzle. The vertical and the horizontal scales for all the traces are identical. For each L_p, the trace corresponds to the value of L_c that produces the maximum excitation amplitude (u_e'/U_e) at the pipe exit centerline. It is clear from figure 2 that the whistler nozzle induces a strong, stable sinusoidal surging of the flow for both laminar (L_p< 15.24 cm) and turbulent (L_p> 30.48 cm) boundary layers at the pipe exit. In the turbulent case (L_p=45.72 cm), only the exit boundary layer is turbulent but the core flow at the pipe exit is nonturbulent. Larger L_p's, in which the pipe exit flow is turbulent over the entire cross-section, also produce stable sinusoidal surging due to this self-excitation. It is apparent from the traces that: the frequency decreases with increasing L_p, the second stage frequency is somewhat lower than that in the first stage for a given U_e and L_p (explained later), the second stage amplitude is lower than that in the first stage, and the peak excitation amplitude in the first stage is the largest for L_p=30.48 cm and decreases for larger or smaller L_p's.

(c) Organ-Pipe Excitation: Even though a monotonic decrease of the self-excitation frequency f with increasing L_p suggests organ-pipe resonance of the nozzle, it was considered important to obtain a direct evidence of this resonance. The u' distribution inside the pipe along the centerline at U_e=45ms^{-1} is shown in figure 3 for a half-wave mode in the first stage of excitation. The wavelength of a full-wave mode was found to be slightly larger than half of the half-wave mode. This is not unexpected because the effective lengths for the two modes are likely to be different and should include corrections due to both the collar length L_c (Hasan & Hussain 1979) and the pipe diameter D (Kinsler & Frey 1962, p201). Data in figure 3 correspond to the condition for which u_e'/U_e is the maximum. The vertical scale is logarithmic in order to accommodate large amplitude variations.

(d) Axial Evolution of the Fundamental: The axial evolution of fundamental amplitude u_f' on the centerline for a number of excitation situations involving different stages are shown in figures 4a,b; x is nondimensionalized by the jet diameter in figure 4a and by the corresponding acoustic wavelength λ_a in figure 4b. In order to provide a meaningful basis for comparison between different cases, all data in figure 4 are for a fixed excitation ampli-

tude u'_e/U_e of 3%, achieved by adjusting L_c (see later). The collar exit location for each curve is identified by a vertical hatched line in figure 4a. Note that the data for L_p=60.96 cm (D = 2.54 cm) are also included. The centerline variation of u'_f depends on the relative contributions of the hydrodynamic (instability) wave and the acoustic wave. For an instability wave-dominated case, the axial distribution of u'_f should be initially exponential. The u'_f distribution is altered significantly from exponential when the contribution of the acoustic wave becomes comparable to or larger than that of the instability wave. This has been demonstrated by Rockwell & Schachenmann (1982, hereinafter referenced as RS) by using a one-dimensional model for an impinging jet on a cavity. Which form of oscillation will occur for a given self-sustained resonance condition is intimately connected with the 'quality factor' Q, which is directly related to the damping of the acoustic mode of the system. Typically, Q for a system is defined as $Q=\omega_n/\Delta\omega$, where ω_n is the resonance frequency (representing the maximum gain), and $\Delta\omega$ is the half-power bandwidth. For the whistler nozzle, the excitation amplitude varies with the collar length L_c, which also changes the frequency of excitation. Thus, from a plot showing the variation of u'_e with L_c (hence frequency), one should be able to calculate a crude Q factor for the whistler nozzle. The estimated values of Q for different whistler nozzle parameters are given in table 1b. A small value of Q should represent the case when the instability wave dominates the acoustic wave (see also RS). The high values of Q (in table 1b) for the whistler nozzle suggest the presence of a strong acoustic wave.

In figure 4(a), the amplitude u'_f drops sharply for all cases between x/D=0 and x/D=0.8 to a minimum value and then rises again. This drop in u'_f is predicted by RS's model for the case when the amplitudes of the acoustic and instability waves are comparable. The near-field dip was observed previously by Pfizenmaier (1973) and Hussain & Zaman (1975), even though this dip was surprisingly absent in the data of Crow & Champagne (1971). Note that the dip in u'_f distribution for different cases occurs at nearly the same location ($x/\lambda_a \cong 0.016$) when plotted against x/λ_a (figure 4b). In figure 4(b), the distance between the first and second dips gives an approximate measure of the disturbance wavelength λ. Based on this wavelength, the relationship between collar length and disturbance wavelength was found to be: $L_c/\lambda=n-c$, where n is the stage of excitation and c=0.5. The value of c varies between different impinging flow geometries. A summary of the L_c/λ

values for different impinging shear layers is given by Ziada & Rockwell (1982).

(e) Dependence on Velocity: Attempts were made to document the variation of the whistler excitation frequency with velocity. For a given L_c as the velocity was increased slowly, the whistler excitation appeared only for a small velocity range after which the tone disappeared with a further increase in U_e. For a few cases, the whistler excitation could be triggered again at a higher velocity. The variation of the excitation frequency with L_c is due to the fact that the effective length of the pipe-collar combination changes with L_c. However, for a fixed L_c, when U_e is changed, the corresponding shear-layer tone frequency does not match one of the organ-pipe mode frequencies. That is why, unlike the jet tone and shear-layer tone phenomena, whistler nozzle excitation cannot be obtained for a fixed L_c at any arbitrary exit velocity.

3.2 Frequency and Amplitude Variation with the Collar Length:

Perhaps the best demonstration of the underlying phenomenon is the dependence of the excitation frequency f on L_c. Since the phenomenon is the coupling of two resonance mechanisms, i.e. the organ-pipe resonance and the shear-layer tone, the frequency jumps must also depend on L_p. The dependence of the excitation frequency and amplitude on L_c are demonstrated for some representative cases in figures 5 and 6. Figures 5(a)-(c) show the variation of f with L_c; figures 6(a)-(c) show the corresponding amplitudes. Only those spectral components with amplitudes within 45dB of the highest peak for each L_p are included.

(a) Laminar and transitional initial conditions: Figures 5(a), 6(a) cover data for L_p=15.24 cm which has a laminar exit boundary layer. Figures 5(b), 6(b) correspond to a transitional exit boundary layer. Consider figures 5(a) and 6(a) for h=0.3175 cm first. Two modes, one half-wave centered at f≅900 Hz and one full-wave centered at f≅1800 Hz, are excited simultaneously for $L_c > L_{cmin}$. With increasing L_c, f decreases. Note that the half-wave mode is considerably stronger (by about 25dB) than the full-wave mode and occurs for a larger range of L_c. The second stage appears for L_c>2.2 cm and lasts for a much longer L_c range than the first stage. Note that the amplitudes near the peak in both stages are nearly equal. Both the half-wave and full-wave mode frequencies in the second stage are lower than those in the first stage. This is to be expected because L_c adds an effective length to

L_p; the effective length is larger for the second stage than for the first stage. Based on our experimental data, the following relationship was obtained (Hasan & Hussain 1979) to predict the whistler frequency f,

$$\frac{f}{a_o n}(L_p + 1.65\,\frac{L_c}{j} + 0.7D) = 1 \qquad (1)$$

where a_o is the acoustic speed, n (= 1/2,1,3/2,...) denotes the mode and j(= 1,2,3...) the stage. The equation (1) is essentially the organ-pipe equation with end corrections. The curve representing equation (1) is not shown in figure 5 for clarity. When external excitation was applied in the absence of the flow, it was not possible to differentiate between the pipe resonance and the settling chamber resonance.

For the larger h(=0.635 cm), there is no dominant first stage, nor any full-wave mode in the second stage (figure 5a). Some humps in the $\tilde{u}$-spectra were detected for values of L_c corresponding to the first stage, but they were discarded on the basis of the amplitude criterion mentioned earlier. In this region, the $\tilde{u}$-signal trace did not show any change from the unexcited situation, nor was there any audible tone. For h=0.3175 cm in the range 1.2 cm<L_c<2 cm, one single spectral peak at approximately the full-wave mode frequency occurs. This intermediate stage, which does not follow the patterns in stages I and II, has a frequency about 10% lower than expected. The variation of u' along the length of the pipe nozzle for this intermediate stage suggested a very weak full-wave mode. Note that with increasing L_c for any mode or stage, the increase in amplitude at the beginning of a stage is more abrupt than the decrease at the end of the stage (figure 6).

In each of the stages, f decreases with a progressive increase of L_c, as to be expected from the characteristics of the shear-layer tone (HZ) or other self-sustained oscillation phenomena. This suggests that the same basic mechanism which is responsible for the shear-layer tone or the jet tone triggers and sustains the whistler nozzle oscillation.

Figures 5(b) and 6(b) show data for the D=2.54 cm pipe-nozzle of L_p=30.48 cm. For both h=0.3175 cm and 0.635 cm, there are two distinct stages of the half-wave mode accompanied by a weaker full-wave mode (figure 5b). Between stages I and II, there is a full-wave mode which corresponds to a shear-layer tone stage but not a whistler nozzle stage. The amplitudes in these shear-layer tone stages are much lower (15-30 dB) than the amplitudes representing a whistler stage (figure 6b). Note that in figure 6(b) data for only h=0.3175 cm have been presented.

(b) Turbulent initial condition: Figure 5(c) and 6(c) show the frequency and amplitude as a function of L_c for D=7.62cm at U_e=36ms^{-1} and 60 ms^{-1} with a fully-developed turbulent boundary layer at the exit at either speed. In figure 6(c), consider the U_e=60 ms^{-1} case first. There are two stages of excitation: one is centered at L_c≅2.6 cm and the other at L_c≅9 cm. Each of these stages is associated with both a half-wave mode and a full-wave mode. Note that for either the full-wave or the half-wave mode, the frequencies in the two stages are nearly equal, the mid-frequency being slightly lower in the second stage than in the first stage (figure 5c). This is analogous to the shear-layer tone phenomenon (see HZ). The second full-wave mode at U_e=60 ms^{-1} (centered at L_c≅4.5 cm) is a shear-layer tone stage (St_θ ~ .01) which is not supported by the pipe resonance and thus is not associated with a half-wave mode. At U_e=36 ms^{-1}, there is only one stage of whistler excitation consisting of simultaneous half-wave and full-wave modes. Note that (for U_e = 60 ms^{-1}) there is no whistler excitation in the range 5cm < L_c < 7cm.

The shear-layer tone-type behavior of the whistler nozzle suggests that the shear layer from the pipe lip rolls up into discrete vortical structures. Detailed profile data show that the pipe-exit boundary layer is fully turbulent for either value of U_e when D=7.62 cm. Thus, in these cases, the initially fully-turbulent shear layer also rolls up into vortical structures. The roll-up and organization of initially fully-turbulent shear layers into discrete vortical structures was first demonstrated by Clark & Hussain (1979) via visualization and ciné films. Recently, the roll up of an initially fully-turbulent plane mixing layer has been demonstrated and the resulting coherent structure details have been educed by Zaman (private communication). This shear-layer tone for a turbulent boundary layer, though much weaker than that for an initially laminar shear layer, is accentuated by the pipe-nozzle resonance if one of its organ-pipe modes matches the shear-layer tone frequency.

In view of the fact that the roll up of the initially turbulent shear layer into discrete coherent structures will have large dispersion in formation distance, strength, etc., the start of the whistler excitation tone is likely to be less abrupt when initially turbulent than when initially laminar. Data in figure 6(c), when compared with those in figures 6(a)-(b), show consistency with this notion. Furthermore, the vortices in the initially turbulent cases are likely to induce weaker feedback and consequently weaker whistler excita-

tion, not only because of diffuse vorticity but also because of phase and amplitude jitter from one structure to another. As figure 6(c) shows, the peak amplitudes are weaker than in the cases when the shear layer is initially laminar; this was found to be always true. For U_e=36 ms^{-1}, the turbulent case amplitude is 10dB lower than that in the laminar case. Note that the rise in amplitude with increasing L_c is sharper for shorter L_c, because at shorter L_c the rolled up vortices are stronger (due to higher coherent vorticity) and thus capable of producing stronger feedback.

From the data of figure 5 it can be summarized that the frequency behavior of whistler nozzle is similar to the shear-layer tone (f decreases with increasing L_c). But the range over which the frequency changes in any stage is very limited, since the requirement for shear-layer tone and organ-pipe resonance can not be satisfied for every L_c. It is found that the shear-layer tone frequency is always a multiple of the fundamental frequency having a St_D value in the range (0.3-0.6) of the 'preferred mode' of the jet (Hussain and Zaman, 1981).

(c) Inter-stage gaps: A difference between the whistler nozzle and the shear-layer tone excitations can be identified from figures 5(a)-(c). In the shear-layer tone phenomenon, there is always an excitation frequency for every value of the lip-wedge distance within its range of operation; one stage always gives way to the next, typically with an overlap range. Since the whistler phenomenon is the congruence of two resonance mechanisms, excitation will occur when the conditions for both resonances are satisfied simultaneously. Clearly, there will be ranges of L_c where conditions for both resonances cannot be satisfied. Because of this reason, there are inter-stage ranges of L_c where whistler nozzle excitation does not occur (see figures 5a-c). However, in these 'dead zones', the shear-layer tone should still occur in the region between the collar and pipe lips. However, compared to the tone induced by a sharp wedge (see HZ), the shear-layer tone will also be considerably weaker.

3.3 Excitation Amplitude at Pipe Exit

The amplitude of whistler excitation depends on U_e, L_p, L_c and h. For a given L_p, h and U_e, the amplitude can be controlled primarily by changing the collar length L_c. Figure 7 gives one typical example of the variation of excitation amplitude u'_e/U_e (at the pipe exit centerline) as a function of L_c; I and II denote the first and second stages. The sensitivity of the amplitude to the step height h is also included in figure 7. Note that when h is

increased, the collar length must also increase in order for the shear layer to impinge on the collar lip. The vortices get correspondingly more diffuse and the tone amplitude is weaker and its rise is less abrupt. Note that in order to produce a given amplitude of excitation, it is preferable to choose an L_c corresponding to the right hand side of a stage because the change in amplitude is more gradual and less sensitive than on the left hand side. Figure 7 shows that the whistler nozzle can be used to introduce controlled excitation of selectable amplitudes by appropriately choosing L_c. It has been shown that the response of the jet to controlled (see I) self-excitation is similar to that of imposed excitations (Zaman & Hussain 1980, Kibens 1980).

3.4 The Shear Layer Characteristics for the Whistler Nozzle Excitation:

The evolution of whistler tone amplitude and phase profiles are shown in figure 8 for the first stage excitation for L_p=30.48 cm, D=2.54 cm, L_c=1.02 cm, and u_e'/U_e=12%. The measurements were made at three different x-stations: two inside the collar (x=0.254 cm and x=0.635 cm) and one outside (x=2.54 cm). The whistler fundamental tone phase and amplitude profiles are given in figures 8(a)-(b), respectively. Because of the backflow problem, the momentum thickness θ_1, for the data in figures 8(a)-(b) was calculated as follows:

$$\theta_1 = \int_{y_{0.95}}^{y_{0.25}} \frac{U}{U_c}\left(1-\frac{U}{U_c}\right)dy$$

That is, the integration was terminated at the y-location where the mean velocity was 0.25 U_c.

Inside the collar, the perturbation phase remains constant for $(y-y_{0.5})/\theta \lesssim -1$ (figure 8a), then increases to a peak and suddenly drops by about π near $(y-y_{0.5})/\theta_1 \approx 2$. These profiles are in qualitative agreement with the shear-layer tone data (HZ). At each value of x, the radial location of the region of maximum phase gradient $(d\phi/dy)_{max}$ coincides with the minimum of the tone amplitude u_f' (figure 8b), consistent with the prediction of the linear spatial stability theory (Michalke 1965). Note that the locations of the u_f' peak and the minimum move towards the jet center with increasing x. In the shear layer tone, the transverse location of the u_f' minimum was the same at different x.

For the convenience of comparison of whistler nozzle data with other experimental and theoretical data, the u_f' data for x=0.254 cm is plotted in figure 8(c) in a different nondimensional transverse coordinate. Also

included in figure 8(c) are Michalke's inviscid theory (for laminar flow) and Rockwell's (private communication) data for organized wave in an impinging turbulent jet. Each curve in figure 8(c) is identified with two Strouhal numbers except for the Michalke's theoretical prediction. The first Strouhal number is based on the exit momentum thickness ($St_{\theta e}$) and the second one is based on the local momentum thickness θ. Note that in the present case θ was calculated as,

$$\theta = \int_{y_{0.95}}^{y_{0.125}} \frac{U}{U_c}\left(1-\frac{U}{U_c}\right)dy,$$

thus partly accounting for the St_θ values being lower than those in the cited references.

Two different cases of Rockwell's data are included: The first case represents the organized wave data for the oscillation dominated by the instability wave (St_θ=.025), and the second case represents the data where instability and acoustic waves have nearly equal amplitudes at separation (St_θ=.041). These two cases are included in order to permit comparison between similar situations. The general agreement of the whistler data with Michalke's theory suggests that the inviscid parallel flow stability theory may be adequate to describe the overall character of the whistler tone amplitude distribution in the axisymmetric mixings layer. On the high-speed side away from the shear layer, the fundamental amplitude in the whistler tone is higher because of the surging of the core flow. The similarity of these data with Rockwell's also suggests that a similar mechanism is at work here.

3.5 Streamwise Phase Variation

Theoretical models for self-sustained oscillation phenomena assume a phase difference of $2\pi(n+c)$ between separation and impingement points; n is the number of wavelengths between these two points. Continued disagreement on the value of c persists between different theories and experiments. Curle (1953) and Powell (1961) predicted the value of c to be equal to 1/4 for jet tone; Crighton & Innes (1981) predict the value of c to be 7/8 for the shear-layer tone. In experiments, RS found c=0 for the impinging jet, and Sarohia (1977) and HZ found c=0.5 for cavity flow and the shear-layer tone, respectively. The presence of an acoustic resonator in the whistler nozzle is expected to affect the value of c even though it is not known why the interaction of the instability wave with a resonator lead to enhanced feedback.

Because of the transverse phase gradient of the organized wave (for example, see Figure 8a), the transverse location for phase measurement is quite critical. For the whistler tone, the phase was measured along the centerline and along the line correpsonding to U/U_c=0.95. Figure 9 shows the phase variations for a variety of whistler nozzle excitation situations, all data were taken at a fixed excitation amplitude u'_e/U_e of 2%. Note that the phase distributions along the centerline (open symbol) and the U/U_c=0.95 line (solid symbol) are not identical. In figure 9, x/L_c=0 and x/L_c=1 repsesent the pipe exit and the collar exit, respectively. The phase of the excited wave remains nearly constant inside the pipe (x/L_c<0) indicating the dominance of the acoustic wave there; small $d\phi/dx$ suggests that the wavelength is much larger than the collar length L_c. Note the high streamwise phase gradient between x/L_c=0 and and x/L_c=1, after which the phase distributions become nearly linear with x. Similar high phase gradient was predicted by RS's one-dimensional model for an impinging cavity flow, where the organized wave is considered to be the superposition of an instability wave and a standing acoustic wave.

For the purely hydrodynamic oscillations one would expect the phase difference between separation and impingement points to be a multiple of $2n\Pi$. This will not hold when an acoustic wave is simultaneously present with the hydrodynamic wave, as one can see in figure 9. In figure 9, the phase difference between stages I and II at the impingement point ranges between Π and 1.5Π; for purely hydrodynamic oscillation this value should be 2Π.

3.6 Phase Velocity and h/λ Relations

Let us represent the disturbance wave as follows:

$$\tilde{u} = \tfrac{1}{2}\hat{u}(y)e^{i(\alpha x-\omega t)} + \text{conjugate},$$

$$= \tfrac{1}{2}\hat{u}(y)e^{i\alpha(x-ct)} + \text{conjugate}, \qquad (2)$$

where $\alpha = \alpha_i + i\alpha_r$ and $c = c_i + ic_r$ and $\omega = \alpha c$ is the circular frequency. The phase velocity v_{ph} is then given by $v_{ph} = \omega/\alpha_r$. Assuming nearly parallel flow, if ϕ denotes the phase of $\tilde{u}$, it is clear that $\alpha_r = d\phi/dx \equiv 2\Pi/\lambda$. Thus, from the streamwise phase gradient, both the wavelength and the phase velocity v_{ph} can be inferred. The phase velocities calculated from the phase distributions of figure 9 are shown in figure 10. Note that the phase velocity v_{ph}, which equals the acoustic speed within the pipe, decreases rapidly with increasing x and approaches an asymptotic value outside the collar. The

rapid drop of the phase velocity with x in figure 10 should give an idea of the location from where onwards the hydrodynamic wave dominates the acoustic wave. Note that the phase velocity v_{ph} reaches constant values around $0.6U_e$ with increasing x. These values are in general agreement with the data of Ko & Davies (1971), Lau et al. (1972), Bradshaw et al. (1964), Petersen (1978) and Hussain & Clark (1981).

In order to estimate the relationship between L_c and λ, the value of λ within the collar would be more meaningful. Because of the large variation of the phase velocity within the collar, it is not possible to have an accurate estimate of λ within the collar. So, an estimate of the wavelength λ in the region ($x/L_c>2$) where v_{ph} becomes nearly constant was made. Based on this λ, the L_c/λ values for different velocities and stages are listed in table 2; these values do not appear to support a simple relationship of the type $L_c/\lambda=n+c$, expected for self-sustained oscillation phenomena. However, if λ is inferred from the distribution of tone amplitude within the collar (see figure 4b), a $L_c/\lambda=n+c$ type relationship appears reasonable.

3.7 Flow Visualization

In an effort to demonstrate that the whistler nozzle excitation is triggered when vortices in the shear layer within the collar interacts with the collar lip, flow visualization was performed by introducing $TiCl_4$ smoke upstream of the pipe-nozzle. When the excitation is present, one would expect to see a vortex at the collar exit especially when the pipe exit is laminar. The visualization was done for L_p=30.48 cm (D=2.54 cm) at U_e=16 ms^{-1}. Natural roll-up of vortices in the unexcited jet takes place at $x/D\sim2$ (figure 11a). Figure 11b shows the condition when whistler excitation is present. For both excited and unexcited conditions, the pipe exit location is shown by an arrow. Flow visualization showed that the shear layer rolls up sooner in x due to the feedback effect during whistler excitation, as should be evident from comparison of figures 11(a) and 11(b). Similar effort to visualize the flow with turbulent initial condition failed to reveal any clear vortex structure. It was not considered worthwhile to visualize the flow within the collar by redesigning the facility with transparent pipes and collars.

3.8. Nondimensional Representation of the Whistler Nozzle Phenomenon:

Nondimensional relationships between the controlling parameters would be helpful in optimum choice of whistler nozzle dimensions and predict its performance in various technological applications. Included among the controlling parameters are: L_p, L_c, D, U_e, and h. Clearly, L_p and L_c are dominant

parameters. Since L_c depends on h, it may not be necessary to include h directly. If the whistler excitation is triggered by a shear-layer tone, which in turn must depend on the instability of the shear-layer (HZ) downstream of the pipe-nozzle, then the phenomenon must depend on the state of the boundary layer at the pipe exit. A length scale of the boundary layer, say the momentum thickness θ_e, must, therefore, be included. Based on our experience with the shear layer tone (HZ), it would appear that nondimensional frequencies $St_c(=fL_c/U_e)$ and $St_{\theta e}(=f\theta_e/U_e)$ would be important characteristic parameters of the whistler nozzle. When St_c vs. L_c was plotted, data did not collapse for different L_p's. However, when the St_c data were plotted against L_c/θ_e, the data collapsed for both L_p=30.48 cm and L_p=15.24 cm (figure 12a); St_c values based on the full-wave mode frequency is also shown in figure 12a. Note that the collapse of the data is comparatively better for the half-wave mode than for the full-wave mode. This collapse suggests that the initial momentum thickness θ_e is an important parameter for the whistler phenomenon and emphasizes the role of the shear-layer tone in the phenomenon.

The variation of St_c with L_c/θ_e is nearly linear; data for different stages fall essentially on the same line. This is not so for the shear-layer tone, the jet tone or other self-sustained oscillations. For the shear-layer tone (HZ) and the cavity flow (Sarohia 1977), St_c varies almost linearly in each stage, but different stages are separated by vertical shifts. In figure 12(a), the first and second stages are not separated and appear to fall on a single line. The nearly linear variation of St_c indicates that even though the shear-layer tone triggers the phenomenon, it is primarily an organ-pipe resonance.

Equation (1) can be used to interpret the results in figure 12. If C_1/j is neglected (i.e. because $C_1/j << L_p/L_c$), and considering the fact that C_2 $D << L_p$, the equation (1) can be approximated as:

$$St_c = \frac{k}{M}\frac{c}{L_p}, \qquad (3)$$

where M is the Mach number. Note that equation (3) predicts a linear variation of St_c with L_c. Note that the collapse of St_c data in figure 12(a) is much better in the first stage than in the second stage because the assumption $C_1/j << L_p/L_c$ is more appropriate in the first stage than in the second stage. From equation (3), one can conclude that the St_θ vs. L_c/θ_e data for different velocities and modes of resonance will not collapse.

Figure 12(b) shows the data of figure 12(a), plotted as St_θ ($=f\theta_e/U_e$) vs. L_c/θ_e. If St_c vs. L_c/θ_e were exactly linear, then St_θ would be a constant. Data in figure 12(b) show that in each stage St_θ decreases with increasing L_c -- a characteristic of the shear-layer tone (HZ). However, unlike in the shear layer tone, the decrease in St_θ with increasing L_c/θ_e is quite gradual, decreasing from about 0.006 to about 0.0045 over the range $0<L_c/\theta_e<250$. The gradual fall off of the St_c values from linear variation with increasing L_c in figure 12(a) and tne corresponding decreasing values of St_θ in figure 12(b) are to be expected because increasing values of L_c produce longer effective lengths of the pipe-nozzle and hence lower excitation frequencies. Because the phenomenon consists of two independent resonance mechanisms, and there are controlling parameters not included in $St_{\theta e}$, it is not expected that $St_{\theta e}$ data will collapse. Even then, it is quite impressive that data for different controlling parameters fall in a narrow band. Note that the tendency for the shear-layer tone stages to fall into separate curves (see HZ) are smoothed by the organ-pipe resonance. The collapse of the data, when non-dimensionalized by θ_e, emphasizes the important role of the shear-layer tone phenomenon in whistler nozzle excitation.

3.9 Whistler Excitation in Pipe-ring and Pipe-hole Configurations:

Our explanation for the whistler nozzle phenomenon was subjected to further scrutiny in ring- and hole-tone configurations. Even though the above data adequately characterize the whistler nozzle behavior as a function of the values of the controlling parameters, these data and their discussions in the foregoing establish well that while the device configuration as well as the control of the excitation amplitude and frequency is extremely simple, the phenomenon is not. The data support our explanation rather well, even though some peculiarities in the details remain unexplained.

Two aspects of the whistler nozzle would negate total success of any simple explanation. Since the phenomenon is the confluence of two independent resonance mechanisms, it is not likely that a simple nondimensional relation can be valid for the entire range of its operation. Such a simple relationship does not necessarily include all controlling parameters; the less-dominant parameters would produce additional deviations from the modeled simple relationship. The second aspect complicating a simple explanation is, of course, the collar. Because of the unavoidable recirculating region (downstream from the pipe exit) within the collar, the whistler tone must produce periodic modulation of the recirculating flow and periodic ingestion of

the ambient fluid. The collar, depending on its length, also alters somewhat the initial condition, i.e. the details of the boundary layer at the exit of the pipe-nozzle. The additional complicating feature of the collar is that its lip does not constitute a sharp edge as is typical in shear-layer tone and jet tone phenomena. Studies with a sharper collar lip were discarded because of the additional complications of the cavity that had to be introduced within the collar in order to produce the sharp lip.

In order to further substantiate our explanation of the phenomenon discussed in the previous sections, it was considered necessary, even highly instructive, to carry out additional experimentations with the whistler nozzle in the absence of the collar. If our explanation was correct, then it should be possible to induce the whistler nozzle excitation in the absence of the collar by placing either a ring or a hole at the location of the collar lip. In either of these configurations, respectively, called pipe-ring and pipe-hole, the recirculating region (which is present for the collar excitation) is eliminated, and there is entrainment of the ambient fluid right from the origin of the mixing layer.

The whistler excitation with a ring and a hole was separately studied with a 2.54 cm diameter pipe-nozzle of length (i.e., L_p=)15.24 cm. In each case, the traversing axis was carefully aligned with the pipe-nozzle axis. A precision cylinder which slides snug into the nozzle as well as the ring or the hole, when in place, was used to check that the ring or the hole axis was aligned with the nozzle axis for all downstream traverses. Both the ring and the hole were held such that the impinging lip was far from the support so that the support did not interfere with the phenomenon. The pipe-nozzle of a thickness of 0.3175 cm was machined square at the downstream end, which thus forced the initial entrainment to be normal to the mainstream (figure 1d) rather than essentially parallel (figure 1e). Detailed data by Husain & Hussain (1979) showed that the two different initial entrainment patterns produce no difference in the time-average measures or instability details of the initial shear layer. In order to record the amplitude and frequency data, the hot-wire was placed slightly downstream of the pipe-nozzle (i.e. x=0.2 cm) and near the high-speed edge of the mixing layer, i.e. U/U_e=.95. This location was chosen such that the sensor was away from the impingement point and yet captured the 'shear-layer tone' in the axisymmetric mixings layer. The ring or the hole will in general induce 'shear-layer tones' in the axisymmetric configuration; only when the shear-layer tone matches an organ-

pipe mode of the pipe-nozzle will a whistler tone be excited. Unless otherwise specified, 'shear tone' in this section will denote those induced by the ring or the hole but not supported by the pipe-nozzle. The latter will be denoted as 'whistler tone'. The measurement probe was inserted through the ring or the hole (figures 1b,c) such that probe-induced shear-layer tone (see HZ) was avoided. In general, the peak amplitudes of the whistler excitation with the ring or the hole were lower than those with the collar. The audible tone was also louder with the collar, indicating that the collar accentuates the sound via the increased radiating surface and enhanced flow surging.

The results of the whistler excitation experiments in the modified configurations involving the ring and the hole are summarized in figures 13 and 14 for three different speeds: U_e=10 ms^{-1}, 24ms^{-1}, and 36 ms^{-1}. Figure 13(a) shows the frequency as a function of the downstream separation b of the hole or the ring from the pipe nozzle. Note that the frequencies fall in three ranges (f ≅ 450 Hz, 1800 Hz, 2600 Hz) denoting the shear tone at the three speeds. However, the whistler tone mode (f ≅ 900 Hz) falls in a small range corresponding to the half-wave mode of the pipe-nozzle. The non-dimensional frequency St_b(=fb/U_e) is shown in figure 13(b). Figure 13(c) shows the frequency data in terms of $St_{\theta e}$ (≡fθ_e/U_e), where θ_e is the exit momentum thickness of the boundary layer.

The data in figure 13 show two trends of the frequency variation with b. For a given U_e, as b is increased, the shear tone frequency f_s should progressively decrease. However, the organ-pipe mode frequency f_p remaining unchanged for a given L_p, the nozzle would tend to limit the shear tone frequency to an organ-pipe frequency. If f_s is significantly different from f_p, the variation of f_s with b will be monotonic. This is the case for U_e=10 ms^{-1}. However, if f_s is close to f_p or its harmonics (which would correspond to higher modes like full-wave, one-and-a-half-wave etc.), then the overall variation of the frequency would be like that of the shear tone. However, there will be ranges of b over which the shear tone frequency will "lock-in" with the organ-pipe tone. In figure 13 the "step-like" f.equency variations are clear; the constant frequency ranges indicate "lock-in." In the non-dimensional coordinates shown in figure 13(c), note that the three distinct shear tone stages in figure 13(a) collapse. The corresponding $St_{\theta e}$ range is 0.01-0.014, agreeing closely with the shear-layer tone data of HZ. Note that there are a total of four shear tone stages, the number of stages increasing with U_e. Note that the shear tone stages in pipe-ring and pipe-hole configu-

rations agree identically with the plane shear-layer tone data of HZ, also shown in figure 13(b). It is quite impressive to find complete collapse of data in stage 2 (see figure 13b) for six different situations.

The whistler tone value of St_b increases linearly with b, the slope of this line decreases with increasing speed. Correspondingly, the $St_{\theta e}$ values are constant for each U_e, the constant value decreasing with increasing U_e.

Note that at $U_e = 10ms^{-1}$ there is a clear shear tone with the ring but none with the hole. This is to be expected because the sharper impinging edge of the ring should produce a stronger feedback. For this reason, U_{emin} for the ring should be smaller than that for the hole; clearly, U_{emin} for the ring is less than $10ms^{-1}$ while it is higher for the hole. There is no corresponding whistler tone at this speed because the ring tone frequency is quite different from the corresponding whistler tone frequency. The b_{min} for the whistler tone with the ring is lower than that with the hole. This is again consistent with the expectation that the feedback from the ring is stronger and thus the tone should occur at a smaller b. Note that at $U_e=36ms^{-1}$, there is even an earlier stage for the pipe-ring than for the pipe-hole.

The shear tone and whistler tone amplitudes as functions of b are shown in Figure 14(a) for $U_e=24ms^{-1}$ and in figure 14(b) for $U_e=36\ ms^{-1}$. The shear tone and whistler tone stages occur fairly independently. At $U_e=24\ ms^{-1}$, the whistler tone amplitude starts being smaller than the shear tone, but reaches rapidly a peak value significantly exceeding the latter. The increasing stages of both shear and whistler tones have decreasing peak amplitudes, because the feedback is weaker at larger L_c. The shear tone and whistler tone amplitudes are both higher for the ring which is expected to produce a stronger feedback in comparison with that for the hole. Note that at $U_e=36ms^{-1}$, the shear tone and whistler tone amplitudes are comparable. The whistler tone is considerably weaker at other values of b and are thus not shown.

3.10 Comparison of Whistler Tone with Pipe-ring and Pipe-hole Tones

The pipe-ring and pipe-hole configurations were examined in order to obtain further support for the explanation proposed by us for the whistler nozzle phenomenon. The data convincingly validate the explanation. Data in figure 12(a) for the whistler tone are consistent with those in figure 13(b) for the pipe-ring and pipe-hole systems; note the linear variations of St_c and St_b with L_c/θ_e and b/θ_e, respectively. For $U_e=36ms^{-1}$, these two variations

are essentially identical; see comparison shown in figure 13(b). There is also an amazing agreement in the $St_{\theta e}$ values; for example, for a value of L_c/θ_e or b/θ_e of about 160, the $St_{\theta e}$ values are essentially identical. Similarly, the St_t values for the fundamental for $b/\theta_e \geq 200$ are essentially the same in figures 12(a) and 13(b). The departure from an exact linear variation in figure 12(a) and from a constant value in figure 12(b) is different from those for pipe-ring and pipe-hole systems. These differences are to be expected. With increasing collar length L_c, the effective length of the pipe also increases and hence the organ-pipe mode frequency decreases, while in case of the pipe-ring or pipe-hole, the organ-pipe length and frequency remain unchanged. The comparatively worse collapse of the data for the collar is also to be expected. Since θ_e continuously varies with the collar length (I), the data will perhaps collapse better if the actual θ_e for each L_c were used. This will be prohibitively time-consuming and cumbersome because of the interference of the collar. That is why the θ_e values used in figures 12(a), (b) are the corresponding unexcited values.

The amplitudes reported in figures 6 and 14 cannot be directly compared because the sensor locations for the whistler nozzle and for the pipe-ring or pipe-hole had to be different. However, the audible tone was much louder for the whistler nozzle than for the pipe-ring or pipe-hole. This is to be expected because of the direct effect of the collar which enhances the flow surging and provides additional sound radiating surfaces.

It should be emphasized that jet excitation is possible without the pipe-nozzle in ring-tone and hole-tone configurations if the initial condition is laminar. When initially turbulent, the pipe nozzle is essential for jet excitation. For initially turbulent shear layers at the exit of a contraction nozzle, self-excitation could not be induced.

Finally, it should be emphasized that the $St_{\theta e}$ values for the full-wave mode of whistler excitation fall in the range 0.009-0.012, representing the shear layer tone (see HZ). However, the dominant mode (typically the half-wave mode) has a lower $St_{\theta e}$ (0.004-0.006). This paradox can be resolved by noting that the jet Strouhal number St_D ($=fD/U_e$) corresponding to the dominant mode nearly corresponds to the 'preferred mode' of the jet (Hussain & Zaman 1981). Table 3 presents approximate St_D values of the dominant whistler excitation for D=3.81cm at high subsonic velocities; the excitation frequencies were measured in the far field with a condenser microphone. Note that the dominant St_D values for all the cases (except for D=7.62,

L_p=30.48 at U_e=36 ms^{-1}) fall within 0.3-0.6. The case having a larger St_D (i.e 0.8) has a weaker coupling (indicated by comparatively lower amplitude). Data in this table suggests that the 'preferred mode' of the jet plays a controlling role also; that is, the coupling of the two resonant mechanisms is tuned to the 'preferred mode' of the jet. In essence, the whistler nozzle phenomenon can be viewed as a coupling of three resonant mechanisms: the shear-layer tone, the organ-pipe resonance of the pipe-nozzle and the 'preferred mode' of the jet.

This research was supported by NASA Lewis research center Grant NAG-3-198. The authors are grateful to Drs. G. H. Koopman and D. Bechert for detailed discussions on the data and reviews of the manuscript.

Table 1a. L_{cmin} values of the whistler nozzle for U_e=36ms^{-1}, D=2.54cm.

L_p(cm)	h(cm)	L_{cmin}(cm)	L_{cmin}/θ_e
15.24	0.3175	0.381	17.47
15.24	0.635	0.762	34.95
30.48	0.3175	0.66	15.64
30.48	0.635	1.016	24.08
60.96	0.3175	0.8128	8.02
60.96	0.635	1.2192	12.02

Table 1b. Approximate values of Q for whistler nozzle excitation.

U_e(ms^{-1})	L_p(cm)	D(cm)	h(cm)	$Q(=\frac{\omega_n}{\Delta\omega})$	Stage
36	15.24	2.54	.3175	32	I
	15.24	"	.3175	14	II
	15.24	"	.635	14	II
	30.48	"	.3175	28	I
	"	"	"	16	II
	"	"	.635	31	I
	"	"	"	15	II
	60.96	"	.3175	37	II
	"	"	.635	32	II
36	30.48	7.62	.635	10	I
60	"	"	"	12	II
60	60.96	"	"	14	I

Table 2. v_{ph} and L_c/λ data for D=7.62 cm.

$U_e(ms^{-1})$	f(Hz)	(Stage)	$\frac{v_{ph}}{U_e}$	L_c/λ
60	434	(I)	.805	.1827
	374	(II)	.675	.891
	416	(I)	.761	.22
	372	(II)	.678	.894
45	392	(II)	.621	.945
	366	(II)	.628	1.06
	244	(I)	.738	.1866
30	392	(II)	.755	.924
	242	(I)	.907	.185
	240	(II)	.619	.895

Table 3. Approximate St_D values of the dominant mode of Excitation.

D(cm)	L_p(cm)	$U_e(ms^{-1})$	St_D
2.54	15.24	36	0.58
	30.48	36	0.33
	60.96	36	0.37
7.62	30.48	36	0.8
	30.48	60	0.51
	60.96	36	0.51
3.81	5.08	127	0.52
	5.08	195	0.53
	10.16	86	0.52
	10.16	127	0.35
	15.24	86	0.38
	15.24	127	0.54
	15.24	195	0.43
	22.86	86	0.56
	20.48	86	0.6
	30.48	127	0.57
	30.48	195	0.42

REFERENCES

Bradshaw, P., Ferriss, D. H. & Johnson, R. F. 1964 J. Fluid Mech. 19, 591.

Clark, A. R. & Hussain, A. K. M. F. 1979 Turbulent Shear Flows (London) p. 2.30.

Coles, D. E. 1962 Rand Corporation Rept. R-403-PR.

Crighton, D. & Innes, D. 1981 A.I.A.A. Paper No. 81-0061.

Crow, S. C. & Champagne, F. H. 1971 J. Fluid Mech. 48, 547.

Curle, N. 1953 Proc. Ray. Soc. A216, 412.

Hasan, M. A. Z. & Hussain, A. K. M. F. 1979 J. Acous. Soc. Am. 65, 1140.

Hasan, M. A. Z. & Hussain, A. K. M. F. 1982 J. Fluid Mech. 115, 59.

Hill, W. G. & Greene, P. R. 1977 J. Fluids Engrg. 99, 520.

Husain, Z. D. & Hussain, A. K. M. F. 1979 A.I.A.A. J. 12, 48.

Hussain, A. K. M. F. 1980 Lecture Notes in Physics (ed. J. Jimenez) 136, 252.

Hussain, A. K. M. F. & Clark, A. R. 1981 J. Fluid Mech. 104, 263.

Hussain, A. K. M. F. & Zaman, K. B. M. Q. 1975, In Proc. 3rd Interagency Symp. on Univ. Res. in Transportation Noise, Univ. of Utah, p. 314.

Hussain, A. K. M. F. & Zaman, K. B. M. Q. 1978 J. Fluid Mech. 87, 349.

Hussain, A. K. M. F. & Zaman, K. B. M. Q. 1981 J. Fluid Mech. 110, 39.

Kibens, V. 1980 A.I.A.A. J. 18, 434.

Karamcheti, K., Bauer, A. E., Shields, W. L., Stegen, G. R. & Woolley, J. P. 1969 N.A.S.A. SP-207, p. 207.

Kinsler, L. E. & Frey, A. R. 1962 Fundamentals of Acoustics, Wiley.

Ko, N. W. M. & Davies, P. O. A. L. 1971 J. Fluid Mech. 50, 49.

Lau, J. C., Fisher, M. J. & Fuchs, H. V. 1972 J. Sound Vib. 22, 379.

Michalke, A. 1965 J. Fluid Mech. 23, 521.

Petersen, R. A. 1978 J. Fluid Mech. 89, 469.

Pfizenmaier, E. 1973 Doktor-Ingenieur thesis, Technische Universität Berlin.

Powell, A. 1961 J. Acoust. Soc. Am. 33, 4.

Rockwell, D. & Naudascher, E. 1979 Ann. Rev. Fluid Mech. 11, 67.

Rockwell, D. & Schachenmann, A. 1982 J. Fluid Mech. 117, 425.

Sarohia, V. 1977 A.I.A.A. J. 15, 984.

Zaman, K. B. M. Q. & Hussain, A. K. M. F. 1980. J. Fluid Mech. 101, 449.

Ziada, S. & Rockwell, D. 1982 J. Fluid Mech. 118, 79.

FIGURE CAPTIONS

Figure 1. Schematics of different experimental configurations: (a) Pipe-collar (b) Pipe-ring, (c) Pipe-hole, (d) transverse entrainment at lip, (e) nearly parallel entrainment at lip. All dimensions are in cm.

Figure 2. Longitudinal velocity $\tilde{u}(t)$-signal traces at the pipe exit centerline for U_e=36ms^{-1} and h=0.3175 cm. Inserts denote L_p, f and stage, respectively.

Figure 3. Longitudinal fluctuation intensity (u') distribution inside the pipe along the centerline for the first stage, f=244Hz, D=7.62 cm, L_p=60.96 cm and U_e=45ms^{-1}.

Figure 4(a). Streamwise distribution of $u'_f(x/D)$ for D=2.54 cm, U_e=36ms^{-1}, h=0.3175 cm, u'_e/U_e=3%. The pipe lengths (cm), first stage (open symbol) and second stage (solid symbol) frequencies (Hz) are: □, 15.24, 924,820; Δ, 30.48,480,476; O, 60.96, 536,516.

Figure 4(b). The data of figure 4(a) as a function of x/λ_a. For symbols see figure 4(a).

Figure 5(a). Variation of whistler nozzle excitation frequency with collar length L_c (cm) for half-wave mode (open symbols) and full-wave mode (solid symbols); L_p=15.24 cm; D=2.54 cm; and U_e=36ms^{-1}. Δ, h=0.3175 cm; O, h=0.635 cm.

Figure 5(b). f vs. L_c data for L_p=30.48 cm, D=2.54 dm, and U_e=36ms^{-1}. For legend and symbol see figure 5(a).

Figure 5(c). f vs. L_c data for L_p=30.48 cm, D=7.62 cm, h=0.635 cm. □, U_e=36 ms^{-1}; ◇, U_e=60 ms^{-1}. For legend see figure 5(a).

Figure 6(a). Variation of amplitude at the pipe exit corresponding to the data in figure 5(a).

Figure 6(b). Variation of amplitude at the pipe exit corresponding to the data in figure 5(b).

Figure 6(c). Variation of amplitude at the pipe exit corresponding to data in figure 5(c).

Figure 7. Variation of pipe-exit fluctuation intensity u'_e/U_e with L_c for L_p=30.48 cm; U_e=36ms^{-1}, and D=2.54 cm. ◆, h=0.3175 cm, ▲, h=0.635 cm.

Figure 8(a). Phase profile across the shear layer for D=2.54 cm, L_p=30.48 cm, f=504 Hz, U_e=36 ms^{-1}, ■, x=0.254 cm; ▲, x=0.635 cm; ●, x=2.54 cm.

Figure 8(b). Profile of u'_I across the shear layer corresponding to the data in figure 8(a).

Figure 8(c). Amplitude profiles for disturbance tone; ————, Whistler (.006, .0135); ---------, Michalke's theory (.017); —— · ——— · ———, Rockwell (.017, .025); —— · · —— · · ——, Rockwell (.0275, .041).

Figure 9. Streamwise phase variation for D=7.62 cm, L_p=30.48 cm along the centerline (open symbols) and along U/U_c=.95 line (solid symbols). The frequency (Hz), stage and velocity (ms^{-1}) are: □, 420,I,45; ∇, 394,I,60; Δ, 372,II,60; ★, 366,II,45.

Figure 10. Streamwise variation of v_{ph}. For symbols see figure 9.

Figure 11. Flow visualization for L_p=30.48cm, D=2.54 cm at U_e=16ms^{-1}: (a) unexcited (L_c=0), (b) excited (L_c≠0). The arrow indicates the location of the pipe exit.

Figure 12(a). Variation of St_c with L_c/θ_e; L_p (cm) and step height (cm) are: □, 15.24,.3175; Δ, 15.24,.635; O, 30.48.3175; ∇, 30.48, .635. Open symbols denote half-wave mode, and solid symbols denote full-wave mode.

Figure 12(b). Variation of $St_{\theta e}$ with L_c/θ_e. For symbols see figure 12(a).

Figure 13(a). Variation of frequency f with separation b for pipe-hole (PH) and pipe-ring (PR) configurations. The velocity (ms^{-1}) and the corresponding configuration are: ★ , 10, PR; Δ, 24, PR; □, 36, PR; ∇, 24, PH; O, 36, PH.

Figure 13(b). St_b vs b/θ_e. For legend see figure 13(a) —— · ——— · ——, Shear-layer tone (HZ); — - - ——— - - ——, Whistler tone with collar.

Figure 13(c). St_θ vs b/θ_e. For legend see figure 13(a).

Figure 14(a). Amplitude variation of whistler tone (dotted line) and shear tone (solid line) for U_e=24ms^{-1}, L_p=15.24 cm, D=2.54cm. (i) pipe-ring, (ii) pipe-hole.

Figure 14(b). Amplitude variation of whistler tone (dotted line) and shear tone (solid line) for U_e=36ms^{-1}, L_p=15.24cm, D=2.54cm. (i) pipe-ring, (ii) pipe-hole.

ORIGINAL PAGE IS
OF POOR QUALITY

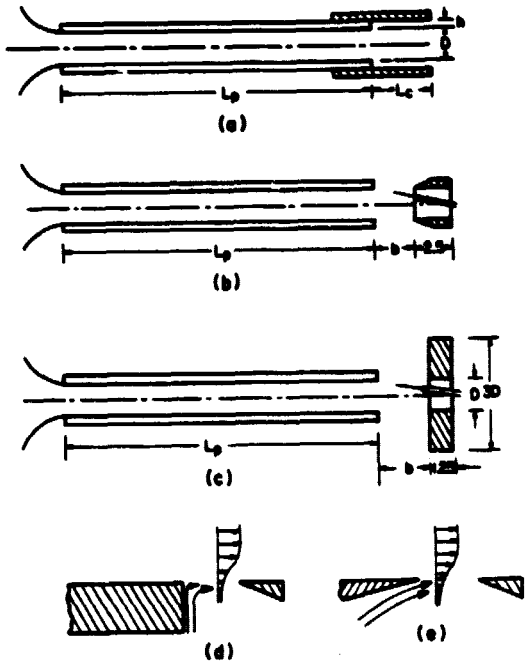

Figure 1

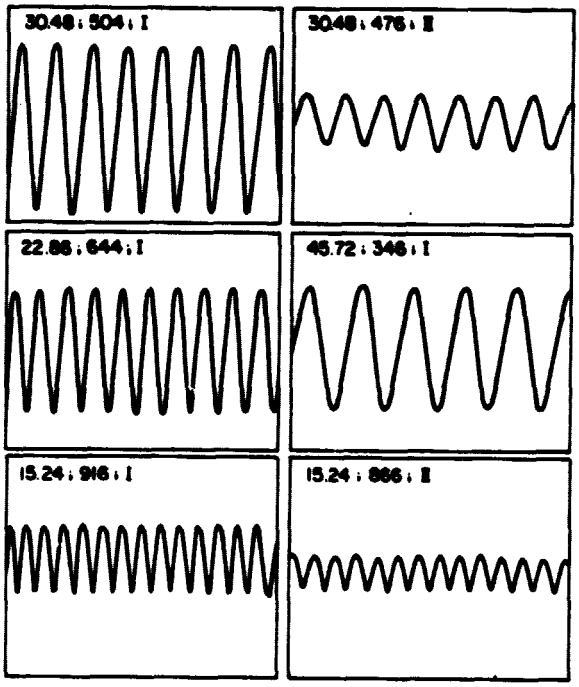

Figure 2

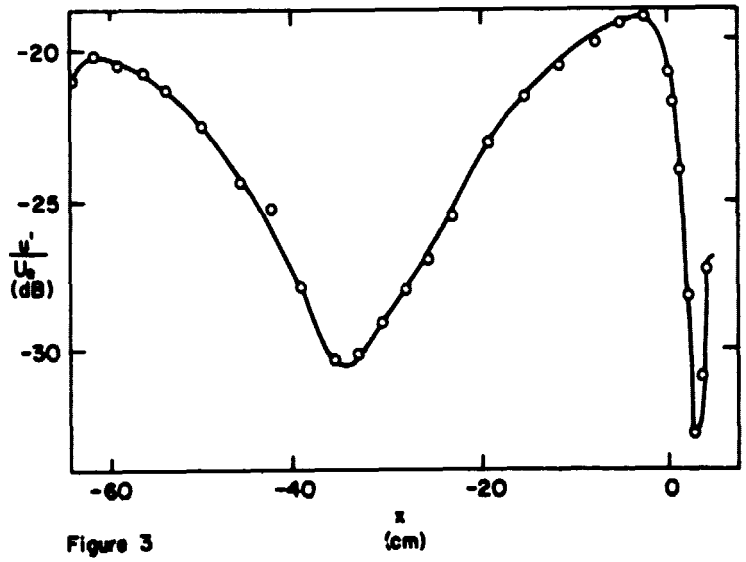

Figure 3

ORIGINAL PAGE IS
OF POOR QUALITY

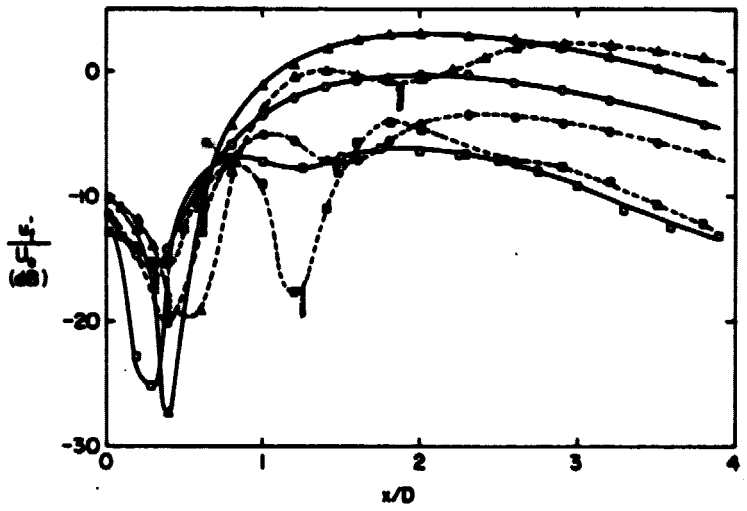

Figure 4a

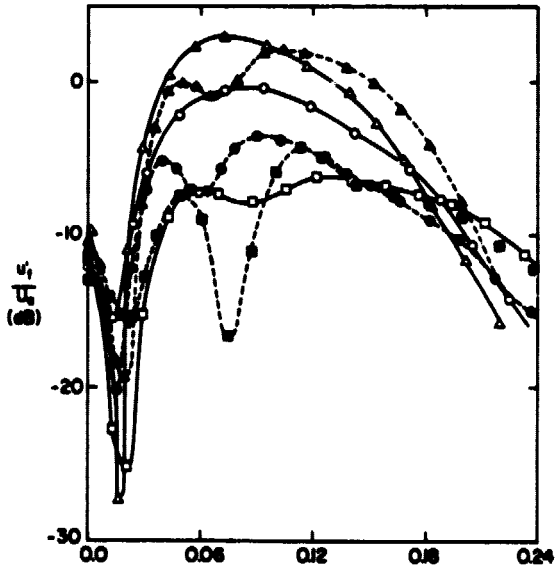

Figure 4b

ORIGINAL PAGE IS
OF POOR QUALITY

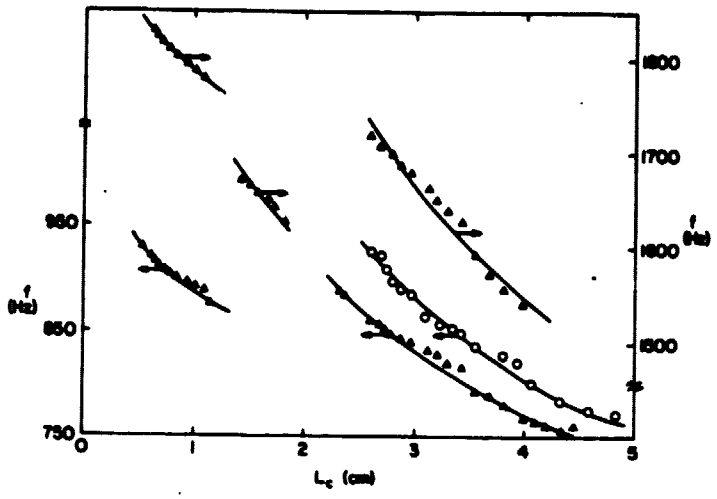

Figure 5a

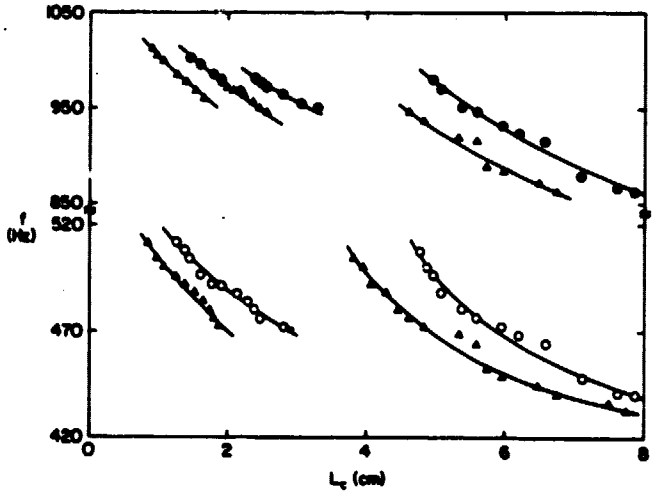

Figure 5b

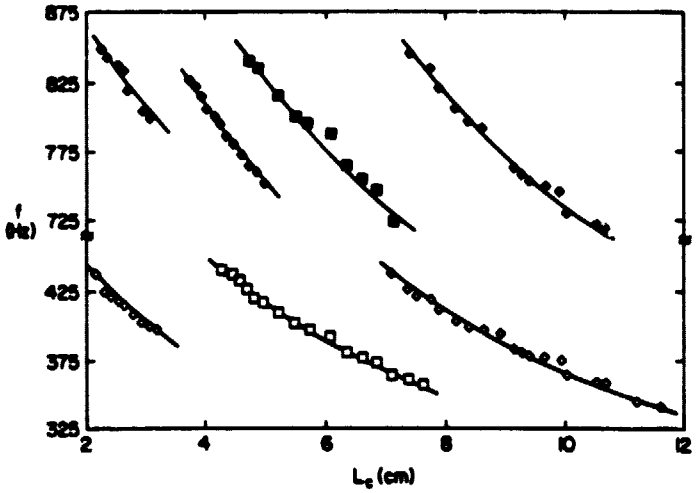

Figure 5c

ORIGINAL PAGE IS
OF POOR QUALITY

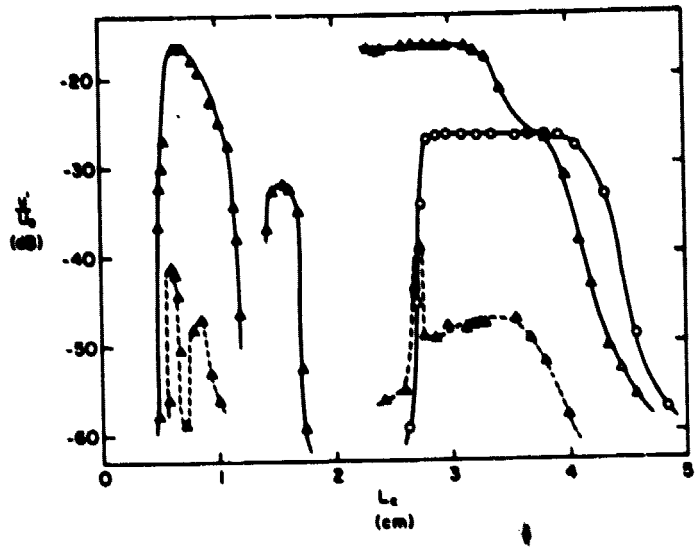

Figure 6a

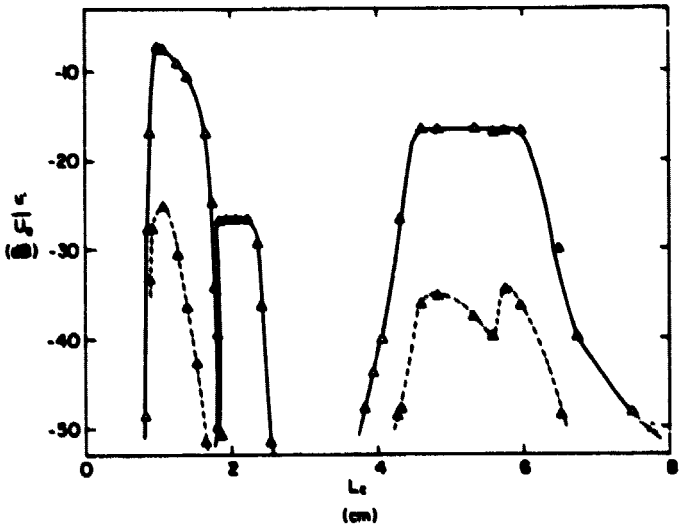

Figure 6b

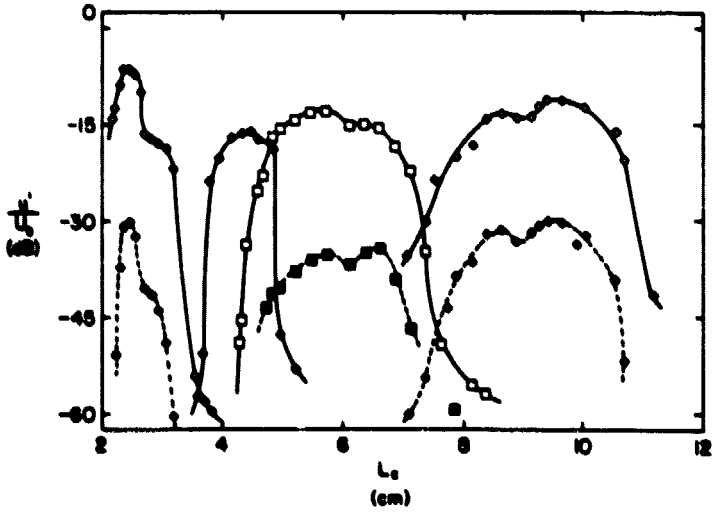

Figure 6c

ORIGINAL PAGE IS
OF POOR QUALITY

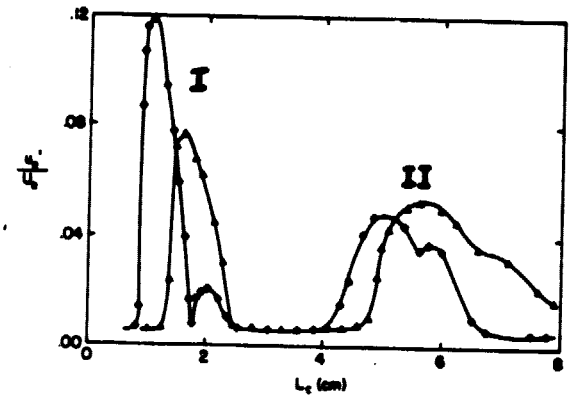

Figure 7

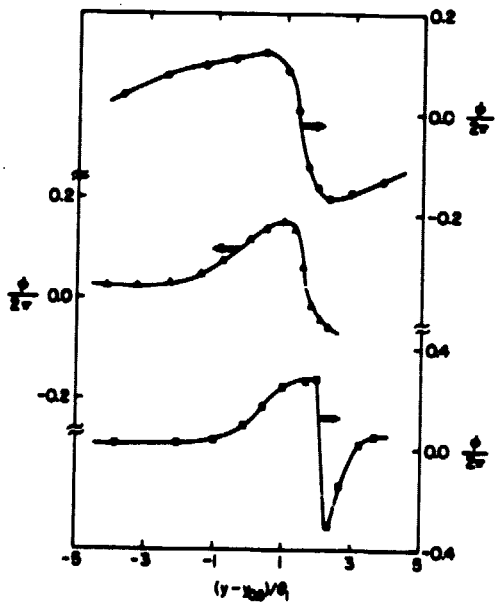

Figure 8a

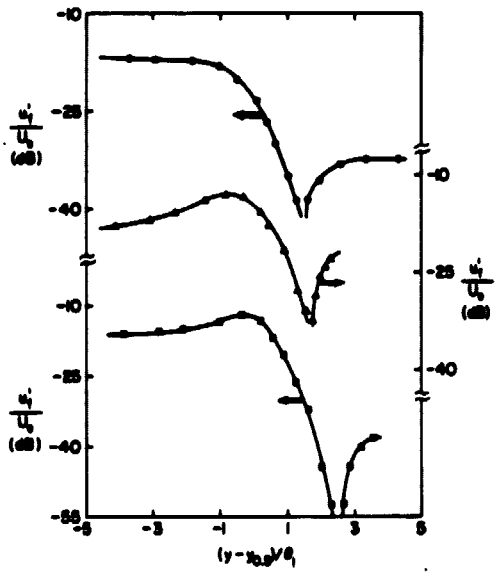

Figure 8b

ORIGINAL PAGE IS
OF POOR QUALITY

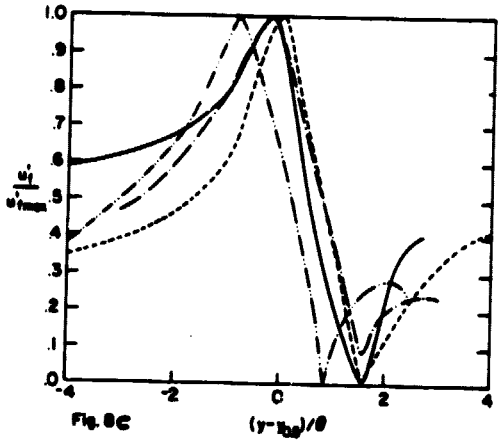

Fig. 8c

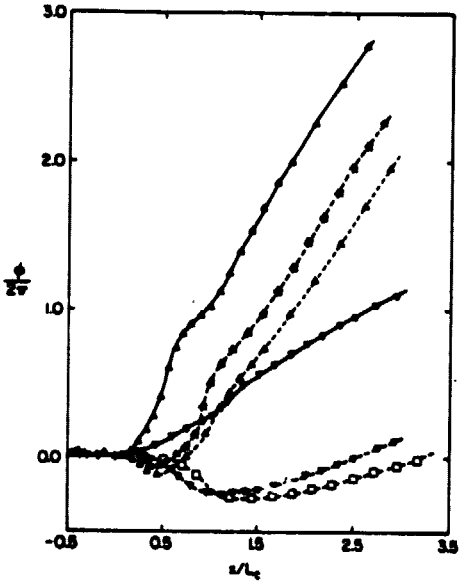

Figure 9

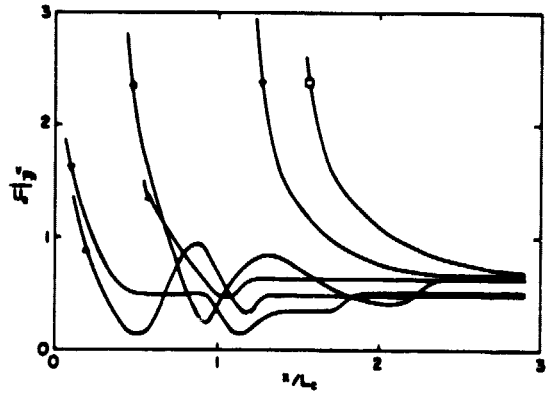

Figure 10

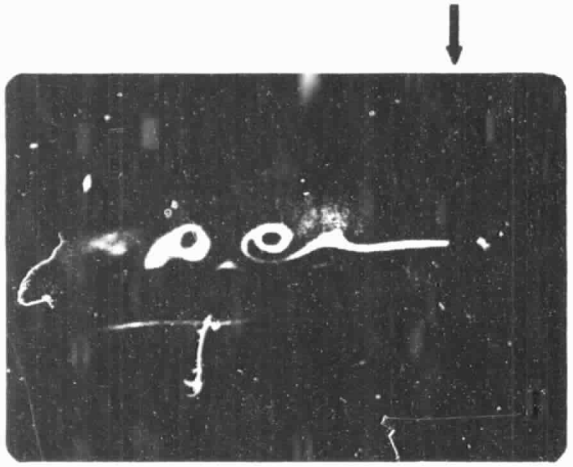

Figure 11(a)

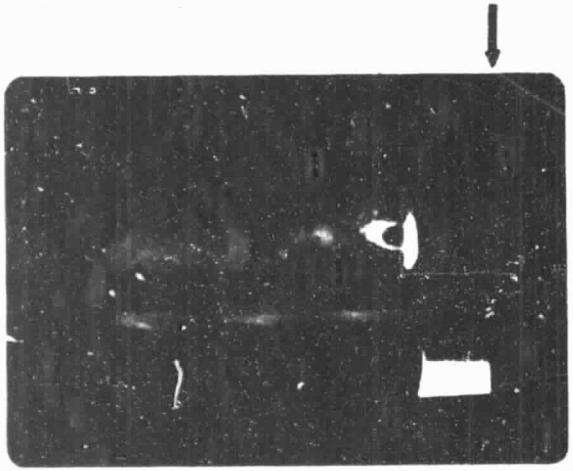

Figure 11(b)

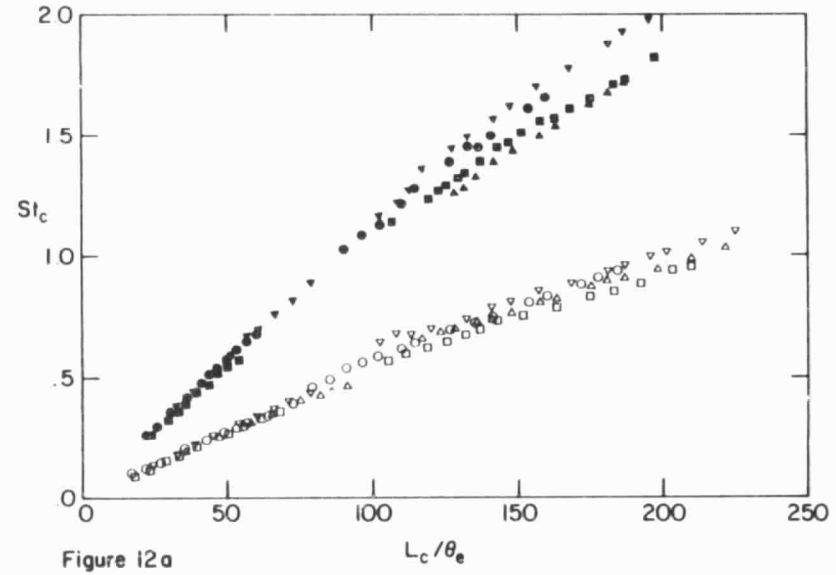

Figure 12a

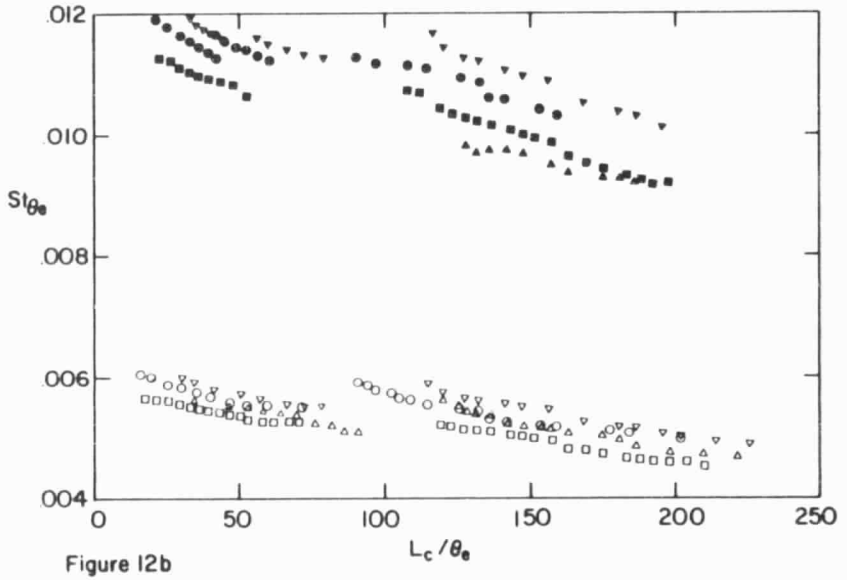

Figure 12b

ORIGINAL PAGE IS
OF POOR QUALITY

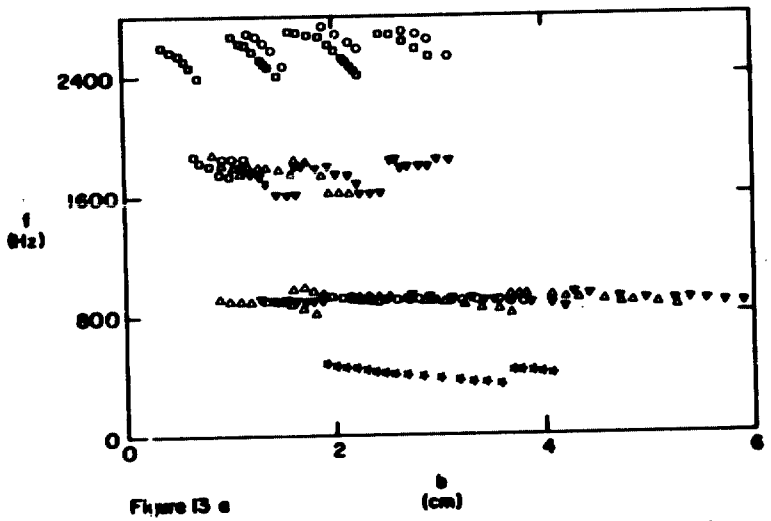

Figure 13 a

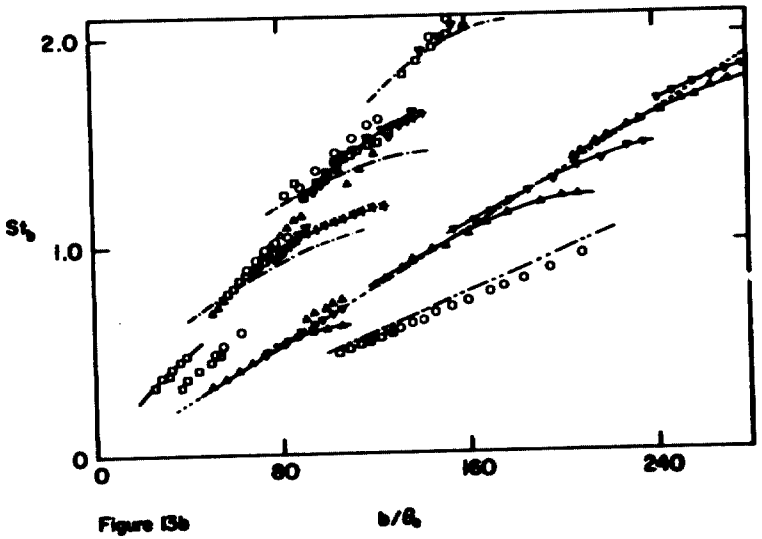

Figure 13b

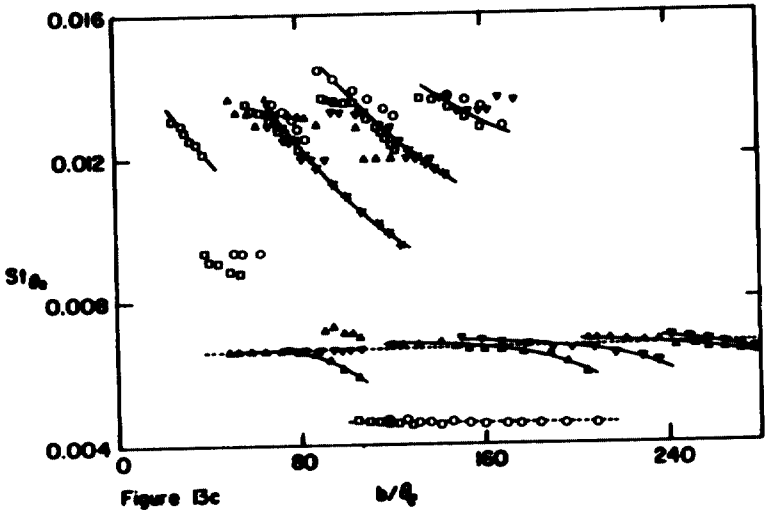

Figure 13c

ORIGINAL PAGE IS
OF POOR QUALITY

ORIGINAL PAGE IS
OF POOR QUALITY

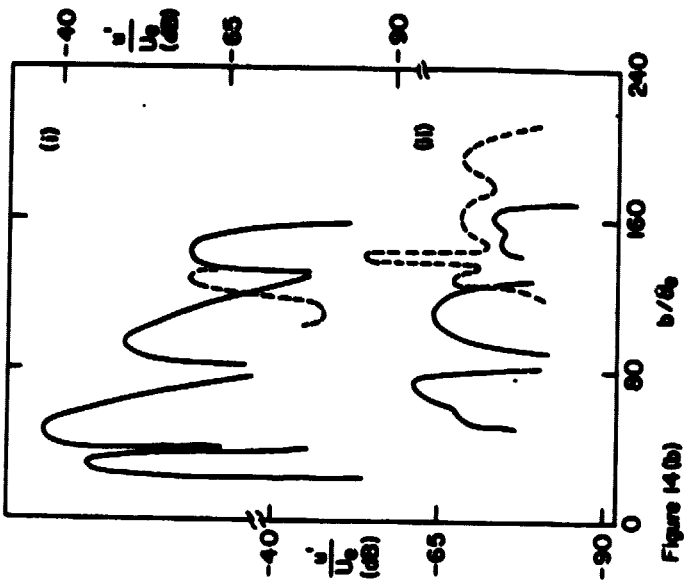

Figure 14(b)

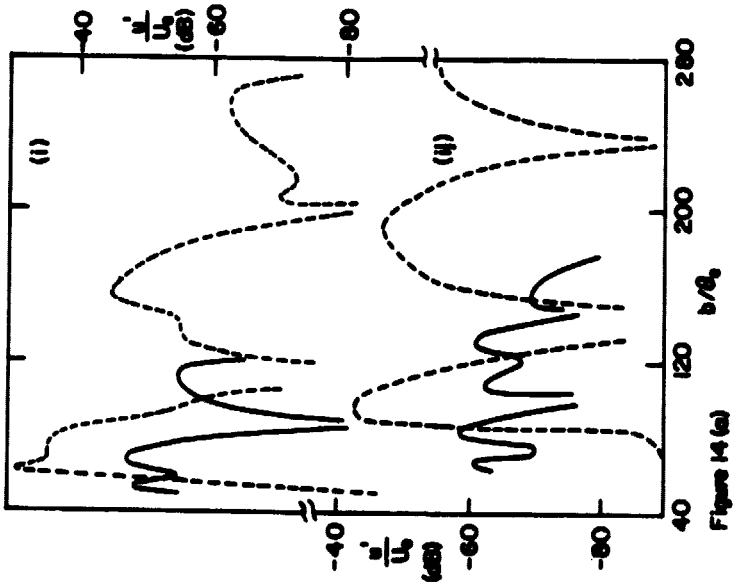

Figure 14(a)